

WESTINGHOUSE CLASS 3

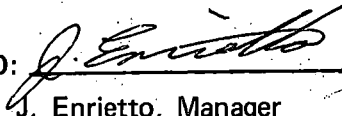
WCAP-9638

METALLURGICAL INVESTIGATION OF  
CRACKS IN THE STEAM GENERATOR  
FEEDWATER LINES OF SURRY STATION NO. 1

L. Albertin  
G. V. Rao  
T. R. Mager

December 1979

APPROVED:



J. Enrietto, Manager  
Material and Mechanical Technology

Work Performed Under Shop Order No. RMN-66374

WESTINGHOUSE ELECTRIC CORPORATION

Nuclear Energy Systems

P. O. Box 355

Pittsburgh, Pennsylvania 15230

8006090396

REGULATORY DOCKET FILE COPY

Docket # 50-280  
Control # 8006090388  
Date 6/03/80 of Document:  
REGULATORY DOCKET FILE

## ABSTRACT

This report describes the results of a metallurgical investigation of the cracking of reducer sections that were part of Loop B and C steam generator feedwater pipes at the Surry No. 1 Nuclear Generating Station of the Virginia Electric and Power Company. The cracks were discovered during ultrasonic and radiographic nondestructive examinations. The metallurgical evaluations included chemistry determinations, tensile testing, impact testing, metallography, and fractography.

Tests showed that the material met the chemistry and strength specification requirements. The ductile-brittle transition temperature for the material was near 25°F with typical Charpy impact values at operating temperature on the order of 190 ft lb. Many cracks were found near the nozzle-to-reducer joint in a machined and tapered section. These cracks generally started from machining grooves and progressed to various depths in the reducers. The largest crack in the Loop B reducer measured 0.080 inches, while the crack depth in the Loop C reducer reached 0.070 inches. Metallographic and fractographic observations suggest that cracking was initially caused by general corrosion at stress concentrations, with subsequent crack growth most likely caused by corrosion fatigue.

## TABLE OF CONTENTS

Section	Title	Page
1	INTRODUCTION	1-1
2	EXAMINATIONS AND TESTS	2-1
2-1.	Surface and Metallurgical Examinations of Sections Containing Pits and Cracks	2-1
2-2.	Metallography	2-1
2-3.	Morphology and Distribution of Cracks	2-1
2-4.	Microstructural Characterization Studies	2-2
2-5.	Fractography	2-2
2-6.	Scanning Electron Microscope (SEM) Fractography	2-2
2-7.	Transmission Electron Replica Microscopy (TEM)	2-2
2-8.	Chemical Analysis	2-3
2-9.	Base Metal	2-3
2-10.	Corrosion Deposits on Crack Surface	2-3
2-11.	Mechanical property Tests	2-3
2-12.	Tensile Tests	2-3
2-13.	Charpy Impact Tests	2-4
3	DISCUSSION	3-1
4	CONCLUSIONS	4-1

## LIST OF ILLUSTRATIONS

Figure	Title	Page
2-1	Cross Section and Inside Diameter Surface Appearance of Reducer B Near the Nozzle-to-Pipe Joint at 121°.	2-5
2-2	Inside Diameter Surface and Cross Section of Reducer B Near Crack Location 64°.	2-6
2-3	Inside Diameter Surface and Cross Section of Reducer B at 227°.	2-7
2-4	Inside Diameter Surface Appearance and Cross Section of Reducer B at 294°.	2-8
2-5	Location and Shape of Cracks at Various Locations in Reducer C (Mag 2x)	2-9
2-6	Metallographic Section Containing the Longest Crack at 121° in Reducer B.	2-10
2-7	Section at 121° Showing Location and Shape of Smaller Cracks Near Weld in Reducer B.	2-11
2-8	Section at 121° Showing Details of Smaller Cracks in Reducer B Near the Nozzle-to-Weld Joint	2-12
2-9	Metallographic Cross Section of Reducer C Showing Several Small Cracks and the Deepest Crack (at 108°)	2-13
2-10	Details of one of the Cracks Shown in Figure 2-9	2-14
2-11	Further Detail of a Second Crack Shown in Figure 2-9	2-15
2-12	Surface Oxidation and Small Oxide Protrusions Found in Reducer B, Section 108°	2-16
2-13	Light Optic Micrographs Showing the Size and Distribution of Ferrite and Pearlite Phases. (Reducer Material, Loop B)	2-17
2-14	Thin Foil Transmission Electron Micrographs of the Reducer Material (Loop B) Showing the Fine Structure in Ferrite Grains	2-18
2-15	Thin Foil Transmission Micrographs of the Reducer (Loop B) Material Showing the Fine Structure and Interlath Spacing of the Pearlite Phase	2-19
2-16	Appearance of the Crack Surface at 64° in Reducer B Before and After Cleaning	2-20

## LIST OF ILLUSTRATIONS (Cont)

Figure	Title	Page
2-17	Appearance of Crack Surface at 108° in Reducer C Before Cleaning	2-21
2-18	Crack Surface at 64° After Cleaning, Reducer B	2-22
2-19	Fractographs Showing the Oxidized and Corroded Surface of Crack at 64° in Reducer B	2-23
2-20	Fractographic Features of Opened Crack at 64° Near Crack tip in Reducer B	2-24
2-21	Fractographs Showing the Oxidized and Corroded Surface of Crack at 108° in Reducer C	2-25
2-22	Fractographic Features of Cleaned Crack at 64° for Reducer B	2-26
2-23	Topographic Features of Crack Surface at 64°, Reducer B, Showing Clusters of Holes Caused by Corrosion Deoxidized by Electrolytic Cleaning	2-27
2-24	Fractographs Showing the Corroded Nature of the Fracture Surface at 64°, Reducer B, Surface Deoxidized by Cleaning	2-28
2-25	Fractographs of Reducer B Crack at 64° Showing a Partially Intergranular Nature of the Fracture; Deoxidized Surface	2-29
2-26	Fractograph Showing the Corroded Nature of the Crack Surface at 108° for Reducer C	2-30
2-27	Additional Fractographic Features Seen on Crack Surface at 108° in Reducer C	2-31
2-28	Fractographic Features Seen at the Crack-Overload Area Transition	2-32
2-29	TEM Fractographs Showing Topographic Features of Crack and Overload Fracture Surfaces in Reducer B at 64°	2-33
2-30	Fractographic Features on Reducer B Crack Surface Resembling Fatigue Striations	2-34
2-31	Crack Deposits Analyzed, and Output Charts of Energy-Dispersive X-rays	2-35
2-32	Charpy V-notch Properties of Reducer B Material in the Test Temperature Range of 100 to 440°F	2-36

## SECTION 1

### INTRODUCTION

This report describes metallurgical investigations to determine the nature and cause of cracking in the steam generator feedwater lines in the Surry No. 1 Nuclear Generating Station of the Virginia Electric and Power Company. The cracks were found during a nondestructive examination of pipe sections near the nozzle-to-pipe joint where similar cracks were detected in other nuclear power plants. The Surry No. 1 Station is a three-loop plant with a generating capacity of 822 MWe. It went into commercial service in 1972.

The feedwater lines A, B, and C connect to the steam generator nozzle via a 16-inch-diameter reducer. The piping is made of Schedule 80 ASTM A106 Gr. B steel, and the nozzle is constructed from A105 steel.

Of the three cracked reducers received for investigation, the one from Loop A was too radioactive to be handled in conventional shops and laboratories and was therefore not used in this investigation. The Loop C reducer was cut too close to the defective area, so that some cracked sections were missing. However, other areas on the reducer were useful so that a partial evaluation was possible.

The main emphasis of the examination was then centered on Loop B and included the following tasks:

- Surface and metallographic examination of various sections containing pits or cracks
- Microstructural characterization studies by light optic and thin foil electron microscopy techniques
- Fractographic examinations of the fracture faces of the cracks
- Chemical analysis of the base material and of the deposits
- Mechanical property tests

The results of these tasks are presented in the following sections.

## SECTION 2

### EXAMINATIONS AND TESTS

#### 2-1. SURFACE AND METALLOGRAPHIC EXAMINATIONS OF SECTIONS CONTAINING PITS AND CRACKS

Prior to cutting various specimens for metallurgical tests, all three reducers were subjected to a nondestructive examination to determine the location and degree of cracking. This examination was done at the Westinghouse Waltz Mill facility using ultrasonic techniques on the cut periphery surface near the nozzle-to-pipe joint. Cracks were reported to be present in all three loops. Looking down from the nozzle towards the reducer and measured clockwise from the top of the reducer at the nozzle end ( $0^{\circ}$ ), cracks were found at locations between  $15^{\circ}$  and  $30^{\circ}$  and between  $90^{\circ}$  and  $120^{\circ}$  in Reducer A, and between  $75^{\circ}$  and  $180^{\circ}$  in Reducer B. Crack positions in Reducer C were between  $330^{\circ}$  and  $15^{\circ}$ , between  $45^{\circ}$  and  $90^{\circ}$ , and between  $210^{\circ}$  and  $315^{\circ}$  locations. The examination indicated that the cracks were not running continuous around the periphery of the reducer but varied in depth and shape. Cut sections from crack locations showed the deepest cracks are located at the "knee" of a machined tapered section below the weld. These deepest cracks measured 0.080 inches in depth at  $121^{\circ}$  in Reducer B and 0.070 in. in depth at position  $108^{\circ}$  in Reducer C. Smaller cracks were found along the tapered section. The profile of the most pronounced cracked sections of Reducer B at  $121^{\circ}$  and  $64^{\circ}$  positions together with the inside diameter surface appearance at the crack area is shown in figures 2-1 and 2-2. Other cross sections of cracked areas in Reducers B and C are shown in figures 2-3 to 2-5.

#### 2-2. METALLOGRAPHY

#### 2-3. Morphology and Distribution of Cracks

Samples containing the largest cracks in Reducers B and C were further evaluated by metallography. Details of these cracks are shown in figures 2-6 to 2-12. Most cracks tend to initiate at stress concentrations such as machining grooves.

## **2-4. Microstructural Characterization Studies**

### **1) Light Microscopy**

Light microscopy was conducted to study the size, morphology and distribution of ferrite and pearlite phases. Figure 2-13 illustrates the typical light micrographs and shows the distribution of pro-eutectoid ferrite and pearlite phases with some banding of pearlite in the major working direction.

### **2) Fine Structure Studies by Thin Foil Electron Microscopy**

The fine structure of the ferrite and pearlite phases was studied by thin foil transmission electron microscopy. Figures 2-14 and 2-15 illustrate the substructures within ferrite and pearlite phases, respectively. No abnormal features are seen. The interlath spacing of pearlite lamellae is estimated to be approximately 0.20 microns.

## **2-5. FRACTOGRAPHY**

### **2-6. Scanning Electron Microscope (SEM) Fractography**

Sections containing some deep cracks (at  $64^\circ$  in Reducer B and  $108^\circ$  in Reducer C) were cut and opened in the laboratory. The appearance of the crack surface from Reducer B before and after cleaning with an electrolytic solution is shown in figures 2-16 and of Reducer C in the as-received condition in figure 2-17. The cleaned surface of Reducer B is shown at higher magnification in figure 2-18. Both the as-received and cleaned crack surfaces were further examined in detail. Fractographic features observed on the as-received surface of the crack in Reducer B are shown in figures 2-19 and 2-20, and those in Reducer C in figure 2-21. Typical fractographs of the cleaned surface (oxide removed) are shown in figures 2-22 to 2-28.

### **2-7. Transmission Electron Replica Microscopy (TEM)**

Transmission electron replica examinations were carried out on one Reducer B cracked surface in order to find any indications of metal fatigue. These indications would be in the form of striations left behind an advancing crack growing by the application of an alternating stress. For this purpose two-stage cellulose acetate-carbon replicas shadowed with platinum carbon were prepared from an opened and cleaned fracture surface at the  $64^\circ$  location. The shadowed carbon replicas were examined with the transmission electron microscope which allows for a better resolution of fracture details at high magnifications. Representative fractographs are shown in figures 2-29 and 2-30. The results are not conclusive. Although some fracture patches resembling fatigue striations were noted, it could not be conclusively shown that these were not produced by the fracture of the pearlite colonies, and hence are not structure related.



## 2-8. CHEMICAL ANALYSIS

### 2-9. Base Metal

A sample of the Loop B reducer was submitted for a chemical analysis to verify that the material composition met the ASTM A106 Gr. B chemical requirements. The results are shown in the table 2-1.

TABLE 2-1  
CHEMICAL ANALYSIS OF LOOP B REDUCER SAMPLE

	Elements, Wt %				
	C	Mn	Si	S	P
Reducer B	0.25	1.03	0.17	0.013	0.006
ASTM A106 Gr. B Requirement	0.3 max	0.29-1.06	0.10 min	0.058 max	0.048 max

### 2-10. Corrosion Deposits on Crack Surface

The corrosion deposits shown in figure 2-31 were analyzed using energy dispersive x-rays. The output of the semiquantitative analysis also shown in this figure indicates that, beside iron oxide, the deposits contained measurable quantities of sulfur and copper.

## 2-11. MECHANICAL PROPERTY TESTS

### 2-12. Tensile Tests

Specimen blanks removed from location 12° and representing the long axis of Reducer B were machined into 0.250-inch round tensile specimens having a 1-inch-gage section. Two specimens each were tested at 75° and 440°F. The results are shown in table 2-2.

TABLE 2-2  
TENSILE PROPERTIES OF REDUCER B

Test Temp., °F	0.2% Offset Yield Strength, psi	Ultimate Tensile Strength, psi	% Elongation in 1 Inch	% Red. of Area
75	40,910	65,660	36.9	71.5
75	41,410	66,160	36.8	70.8
440	31,310	61,620	32.6	70.8
440	31,820	63,130	32.2	68.2

### **2-13. Charpy Impact Tests**

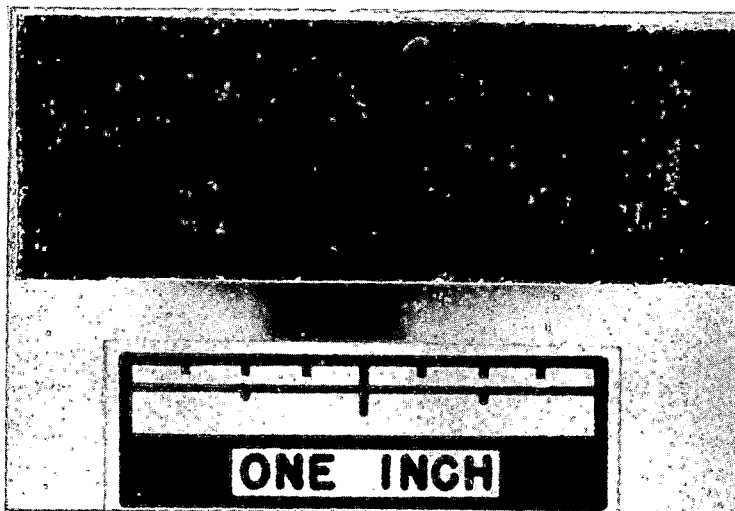
Ten Charpy impact specimen blanks were cut from Reducer B, location 121°, in such a way that the notch plane in the Charpy specimens would correspond to the crack plane of the field fracture. Machined specimens were then tested at various temperatures to determine the ductile-brittle behavior of the steel. The results are shown in figure 2-32.

Weld



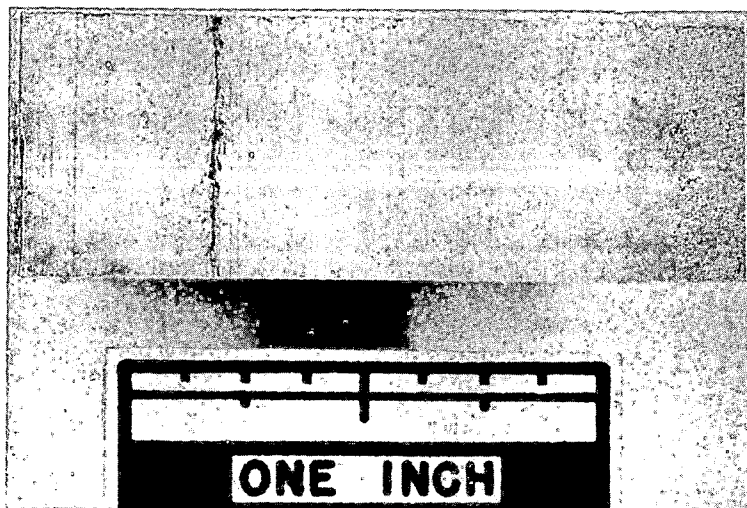
Polished Cross Section

Mag. 2x



As-received ID surface at crack

Mag. 2.5x



Cleaned ID surface at crack

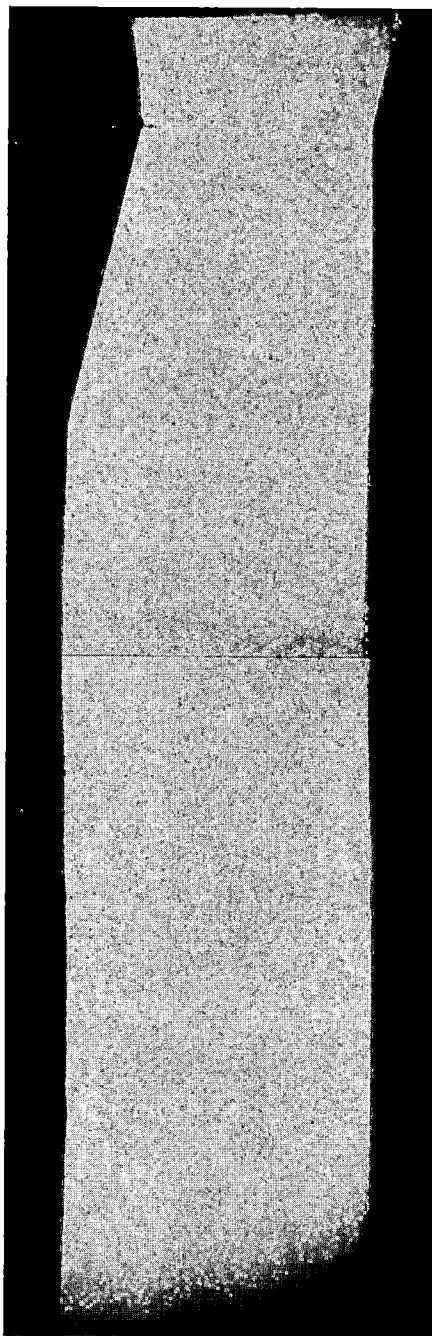
Mag. 2.5x

Figure 2-1. Cross Section and Inside Diameter Surface Appearance of Reducer B Near the Nozzle-to-Pipe Joint at 121°. Note machining grooves and heavy pitting at crack.



ID  
(cleaned)

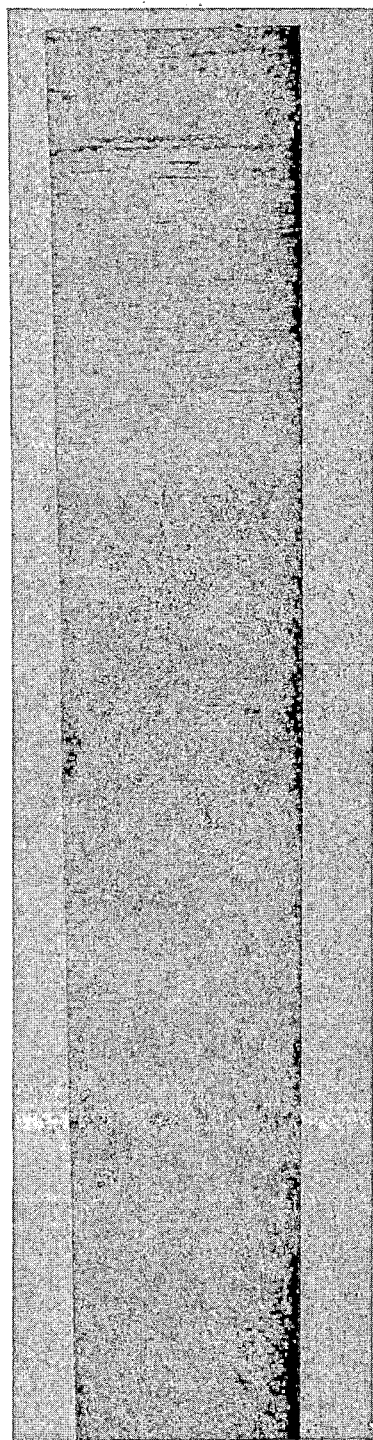
Mag. 2x



ID

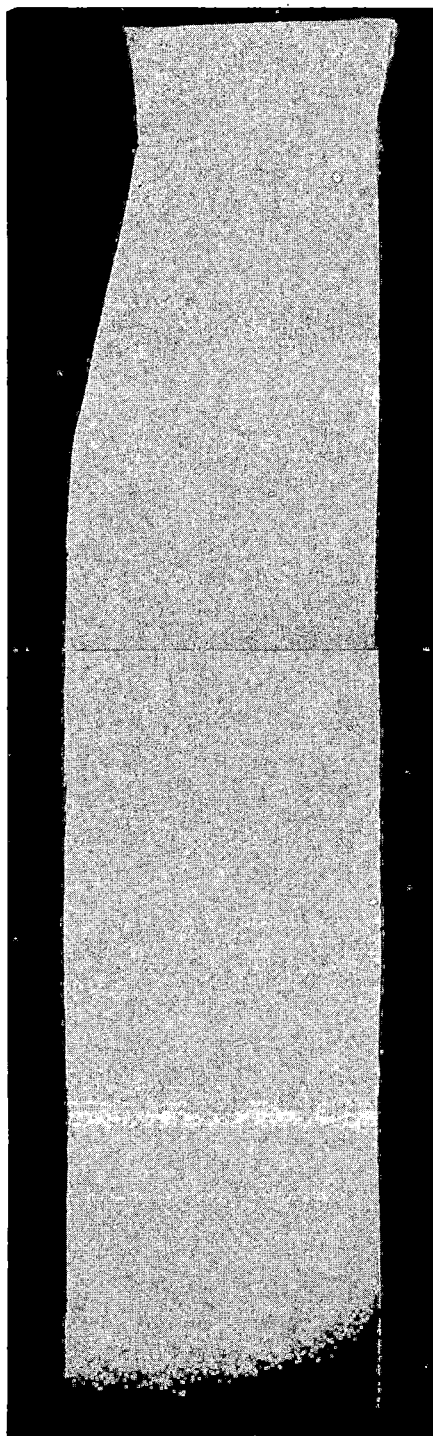
Mag. 2x

Figure 2-2. Inside Diameter Surface and Cross Section of Reducer B Near Crack Location 64 Degrees



ID  
(cleaned)

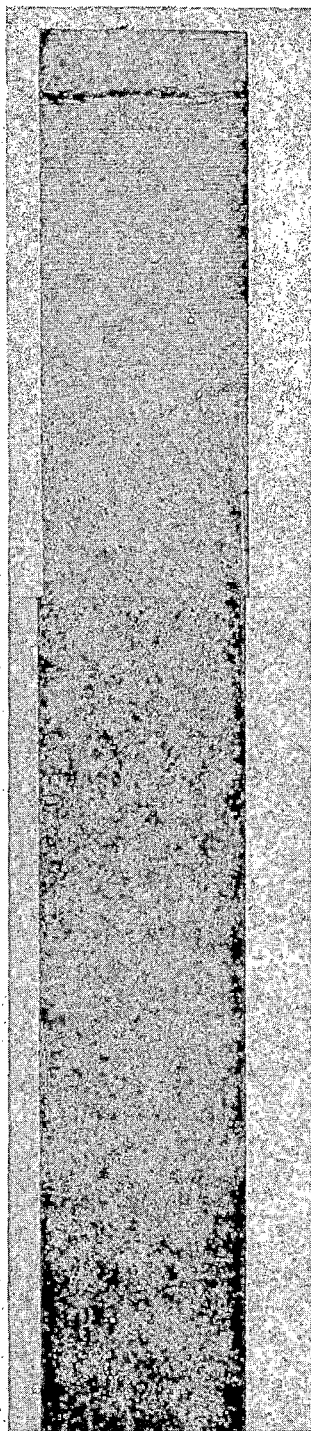
Mag. 2x



ID

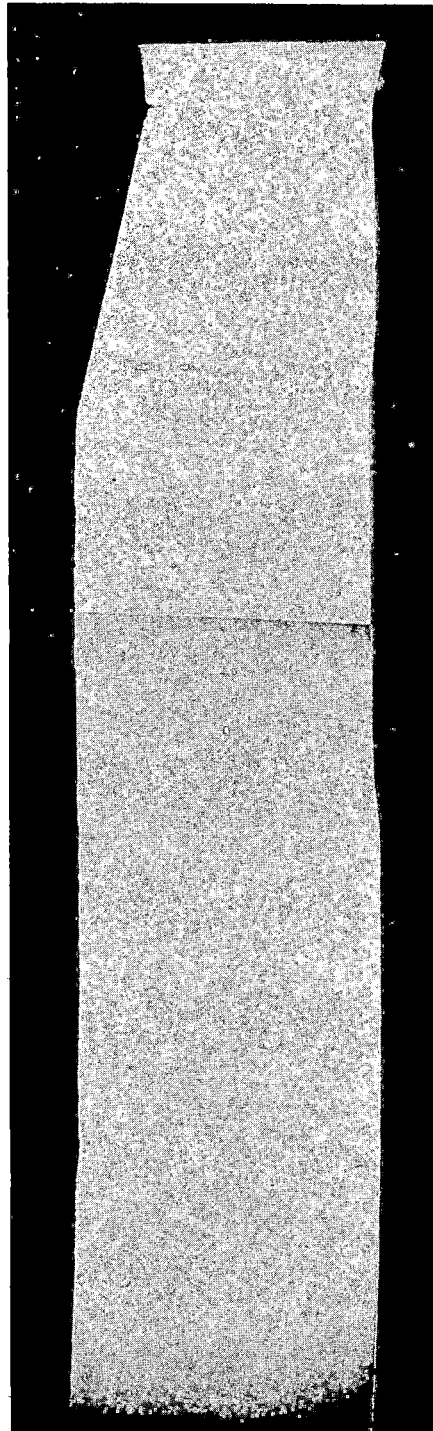
Mag. 2x

Figure 2-3. Inside Diameter Surface and Cross Section of Reducer B at 227°



ID  
(cleaned)

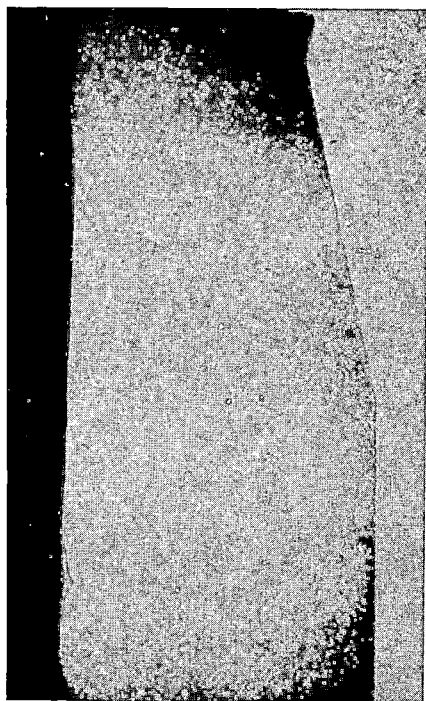
Mag. 2x



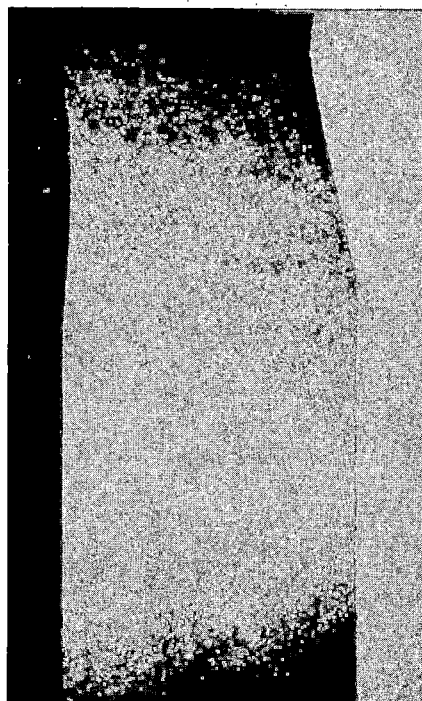
ID

Mag. 2x

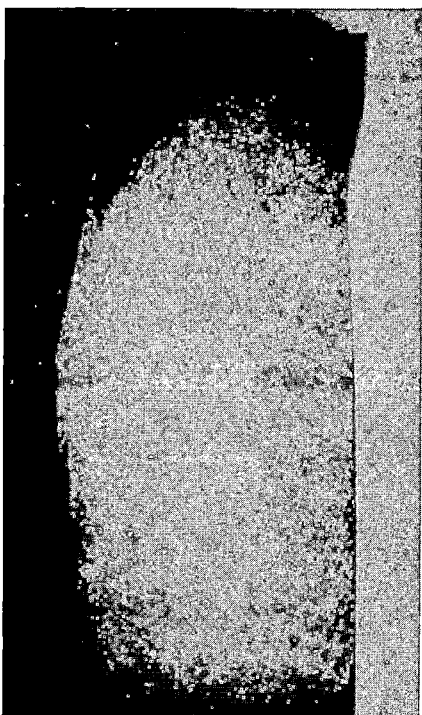
Figure 2-4. Inside Diameter Surface Appearance and Cross Section of Reducer B at 294°



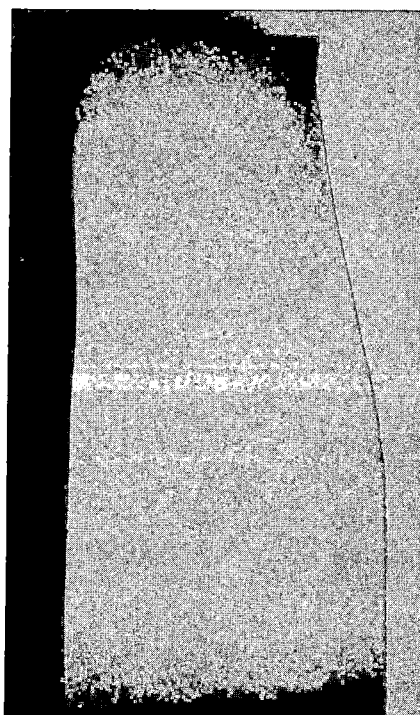
0°



22°

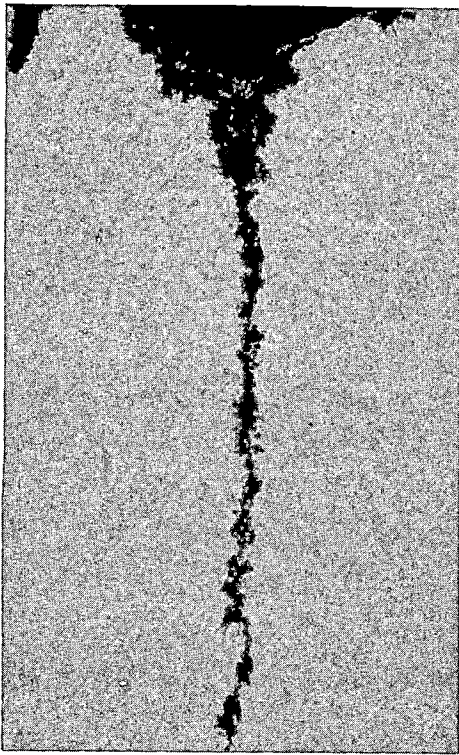


40°



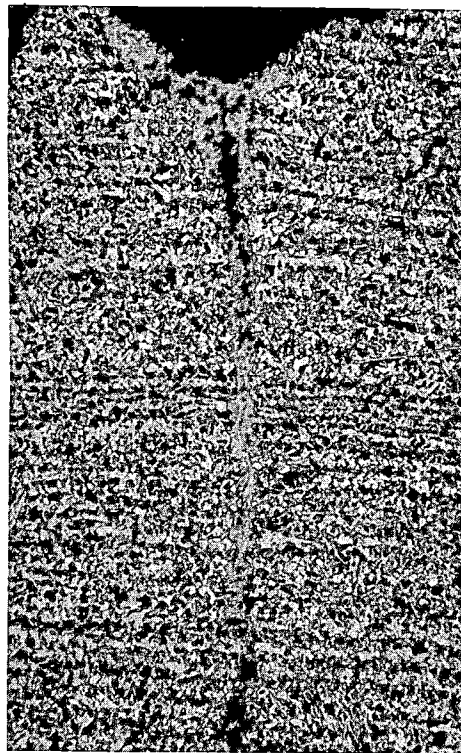
277°

Figure 2-5. Location and Shape of Cracks at Various Locations in Reducer C (Mag. 2x)



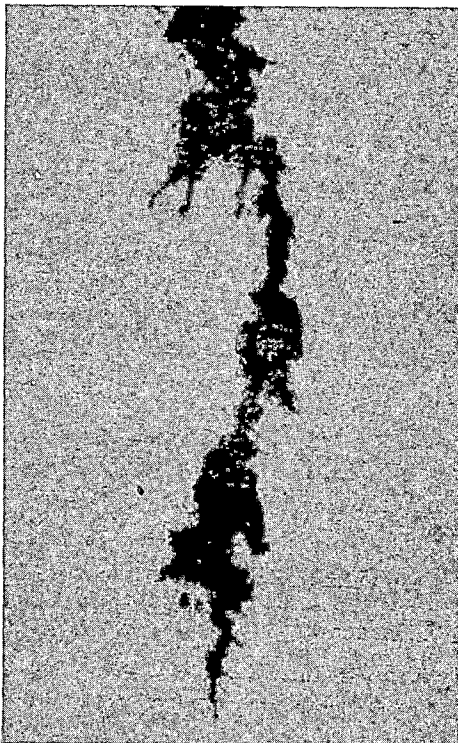
Unetched

Mag. 50x



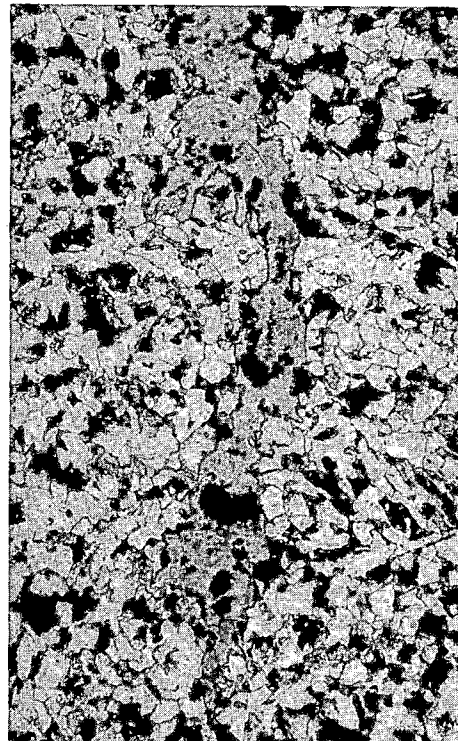
Etched (2% Nital)

Mag. 50x



Unetched

Mag. 200x

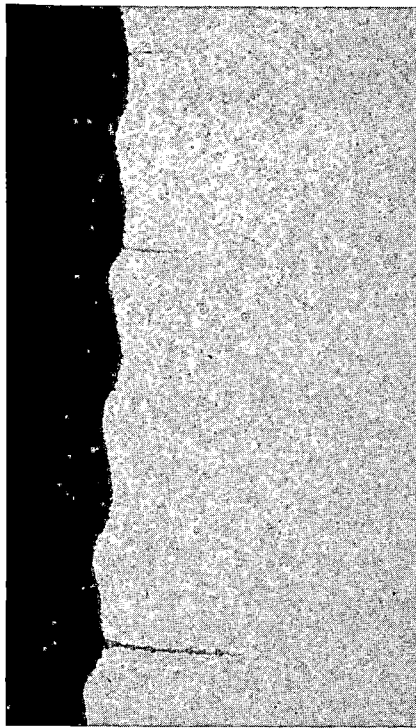


Etched (2% Nital)

Mag. 200x

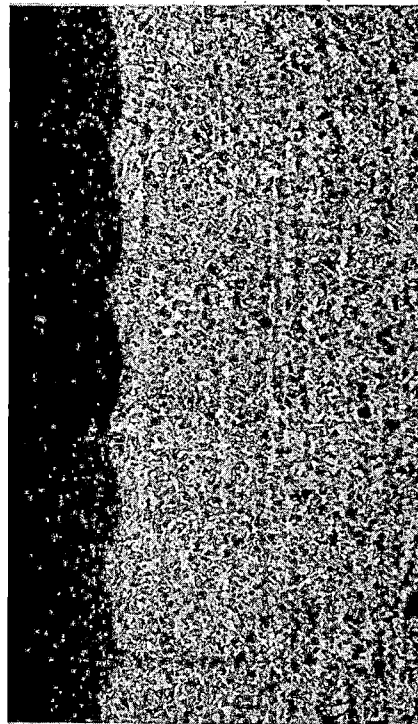
Figure 2-6. Metallographic Section Containing the Longest Crack at 121° in Reducer B. Lower photographs are details of the crack tip.





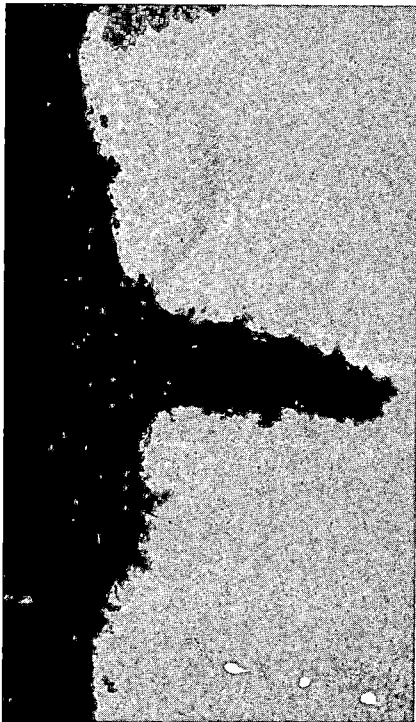
Unetched

Mag. 50x



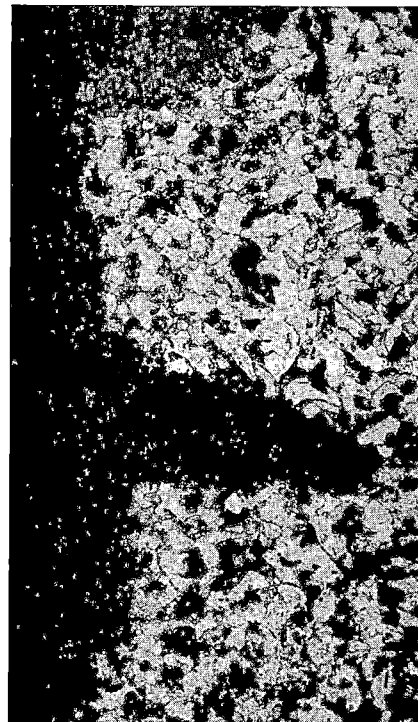
Etched (2% Nital)

Mag. 50x



Unetched

Mag. 200x



Etched

Mag. 200x

Figure 2-7. Section at 121° Showing Location and Shape of Smaller Cracks Near Weld in Reducer B



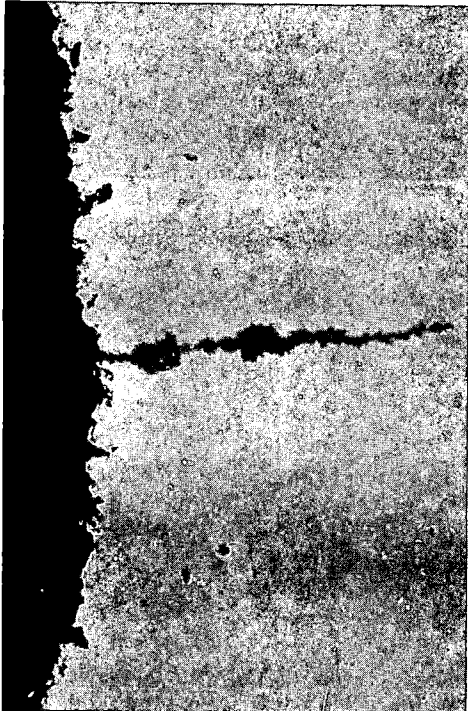
Unetched

Mag. 200x



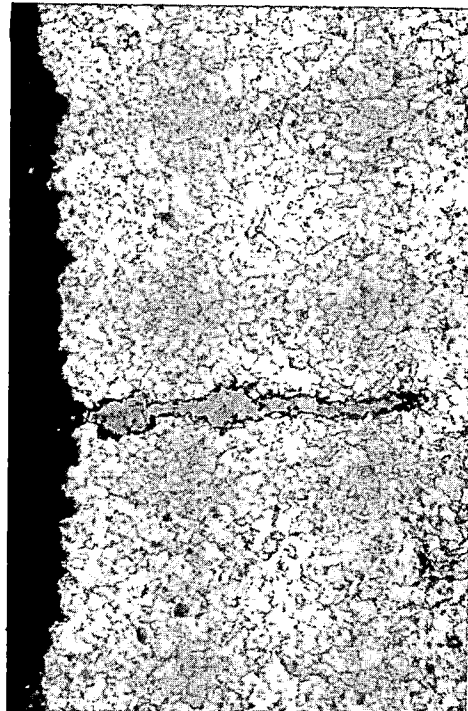
Etched (2% Nital)

Mag. 200x



Unetched

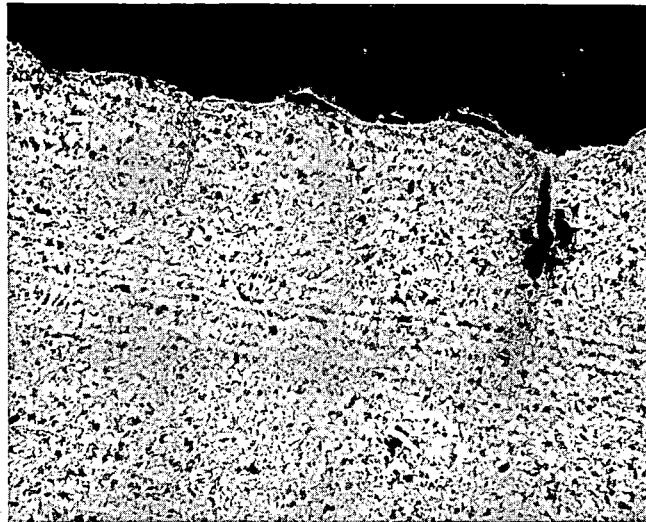
Mag. 500x



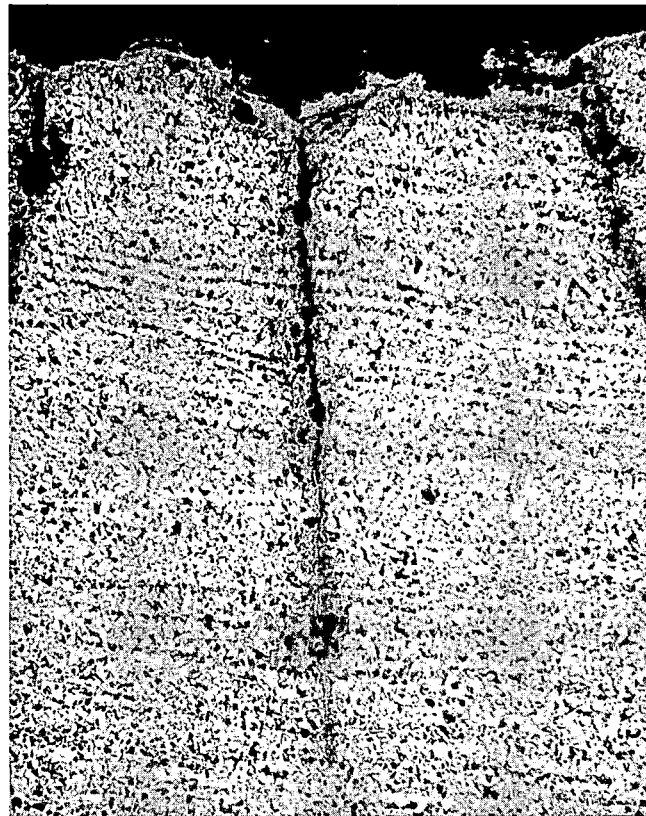
Etched

Mag. 500x

Figure 2-8. Section at 121° Showing Details of Smaller Cracks in Reducer B Near the Nozzle-to-Weld Joint

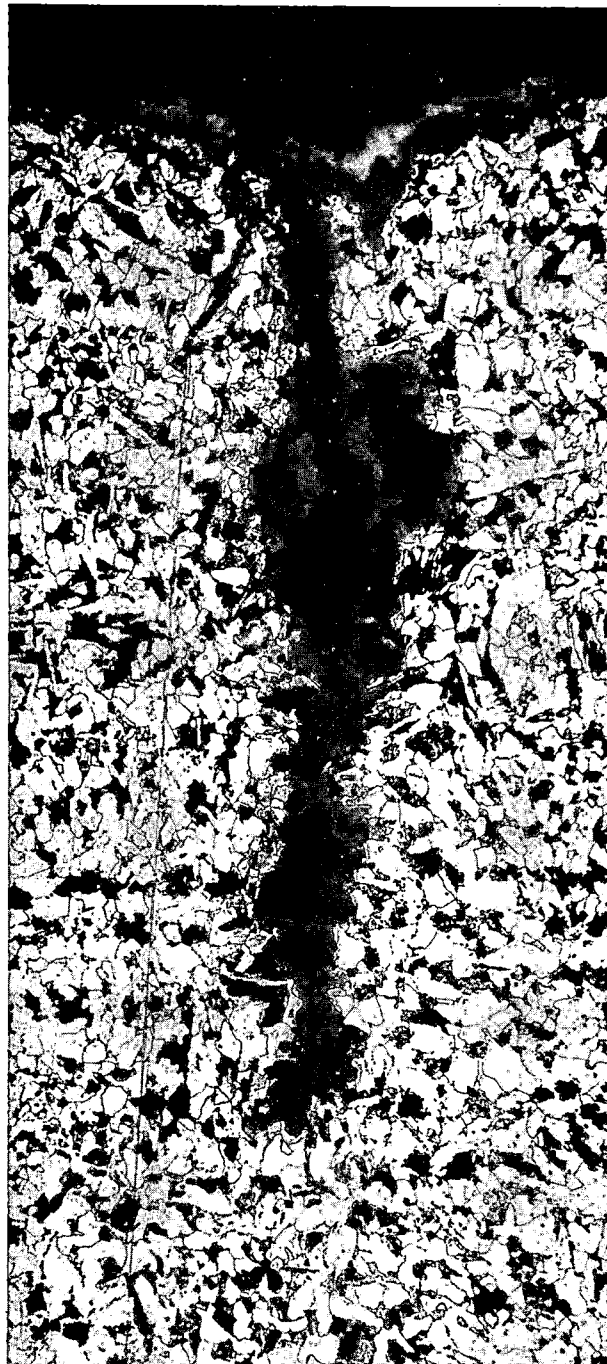


Mag. 50x



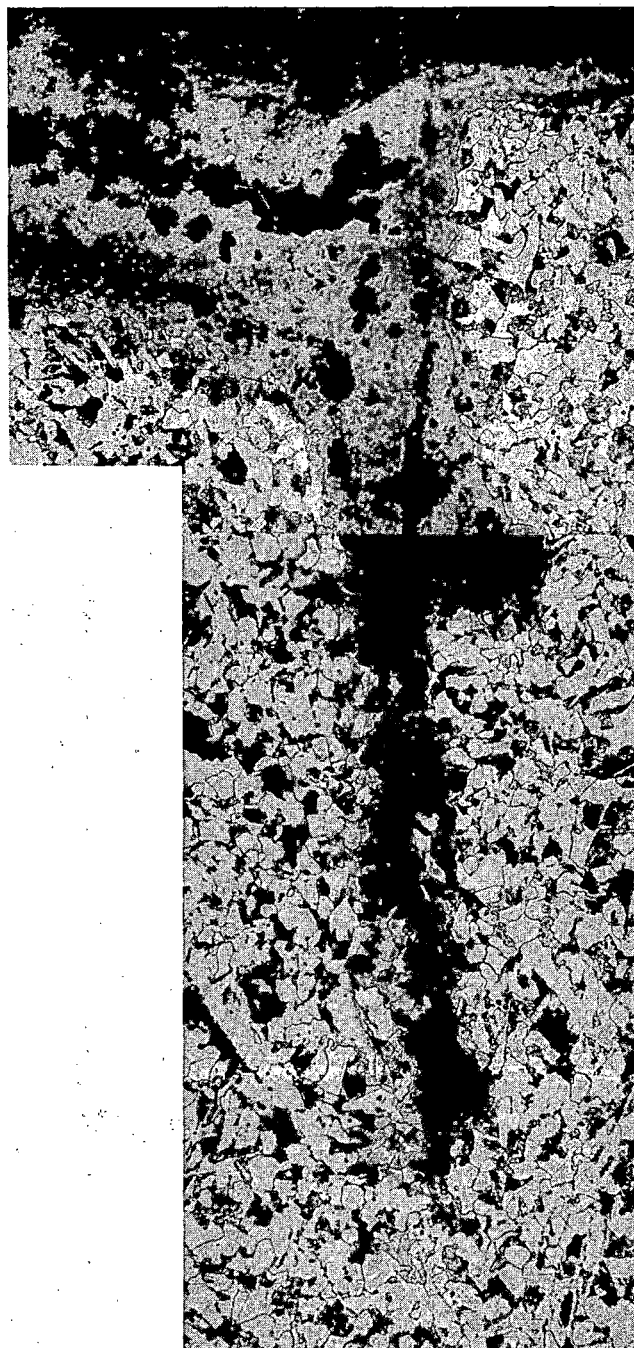
Mag. 50x

**Figure 2-9.** Metallographic Cross Section of Reducer C Showing Several Small Cracks and the Deepest Crack (at 108°)



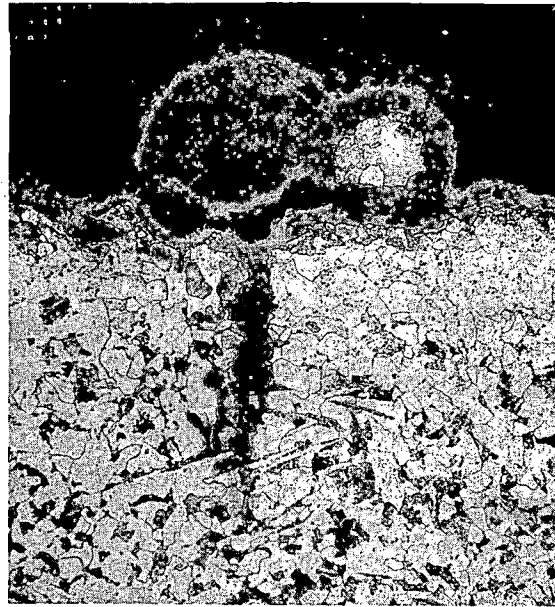
Mag. 200x

Figure 2-10. Details of One of the Cracks Shown in Figure 2-9

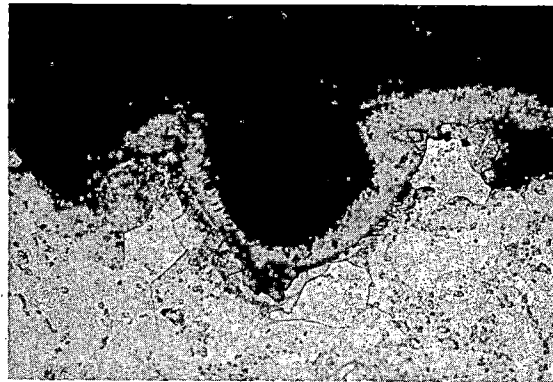


Mag. 200x

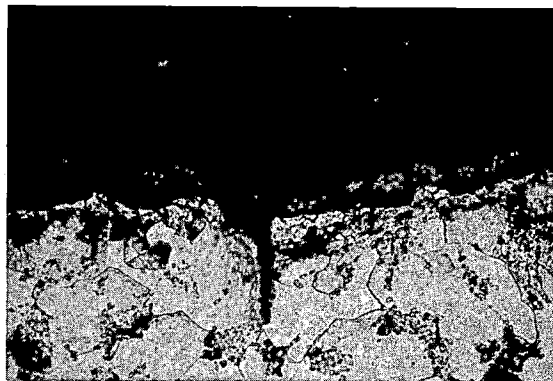
**Figure 2-11. Further Detail of a Second Crack Shown in Figure 2-9**



Mag. 200x

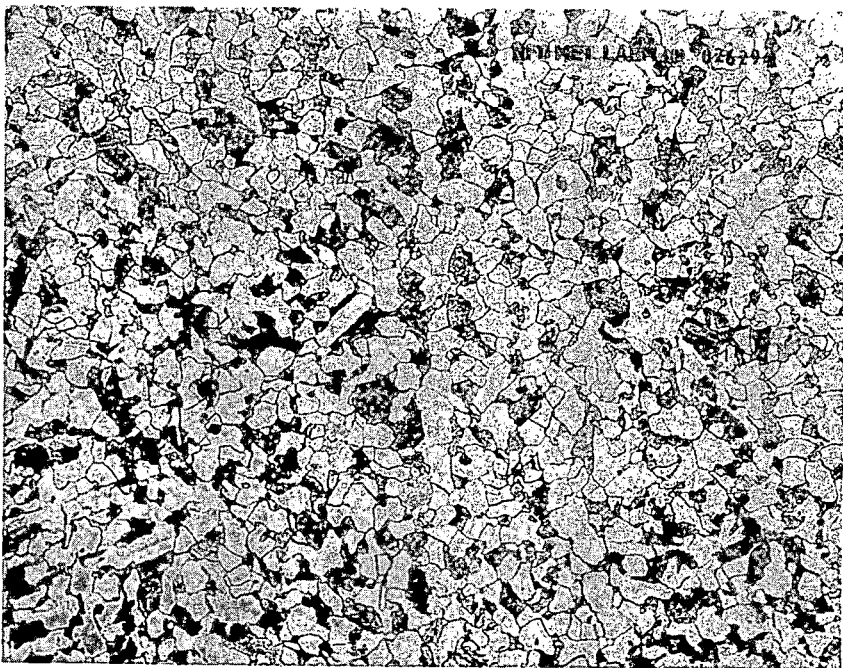


Mag. 500x



Mag. 500x

**Figure 2-12. Surface Oxidation and Small Oxide Protrusions Found in Reducer B, Section 108 Degrees**

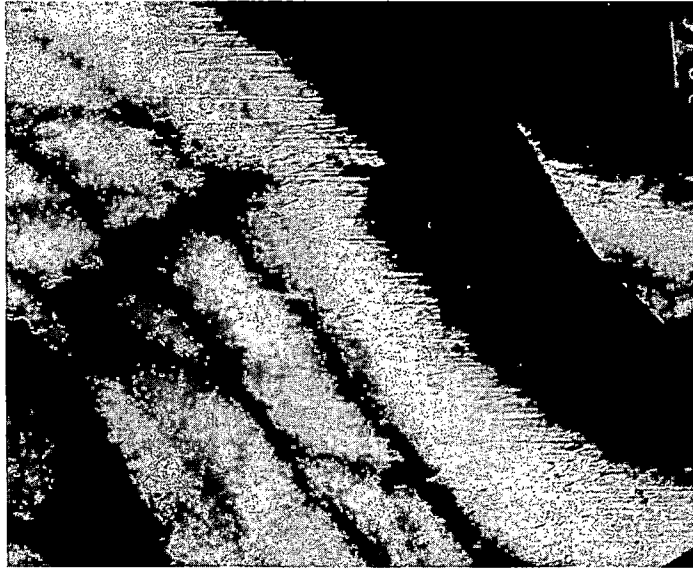


Mag. 200x



Mag. 500x

Figure 2-13. Light Optic Micrographs Showing the Size and Distribution of Ferrite and Pearlite Phases. (Reducer Material, Loop B)



Mag. 12,000x



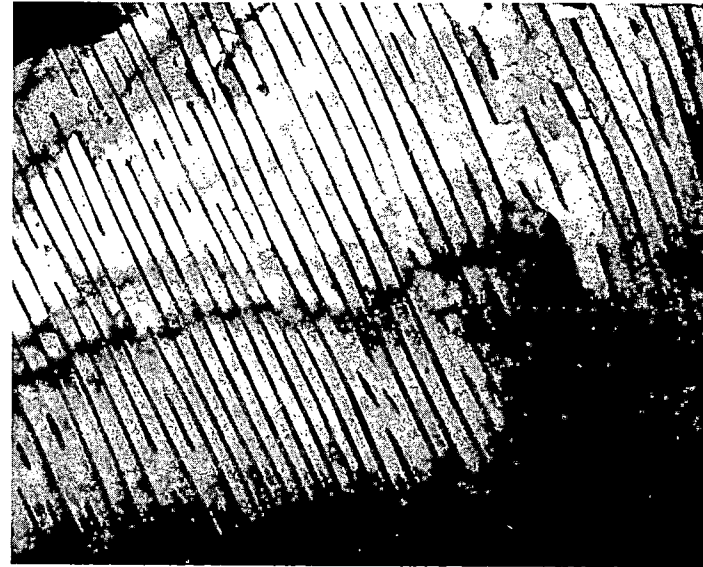
Mag. 12,000x

Figure 2-14. Thin Foil Transmission Electron Micrographs of the Reducer Material (Loop B) Showing the Fine Structure in Ferrite Grains



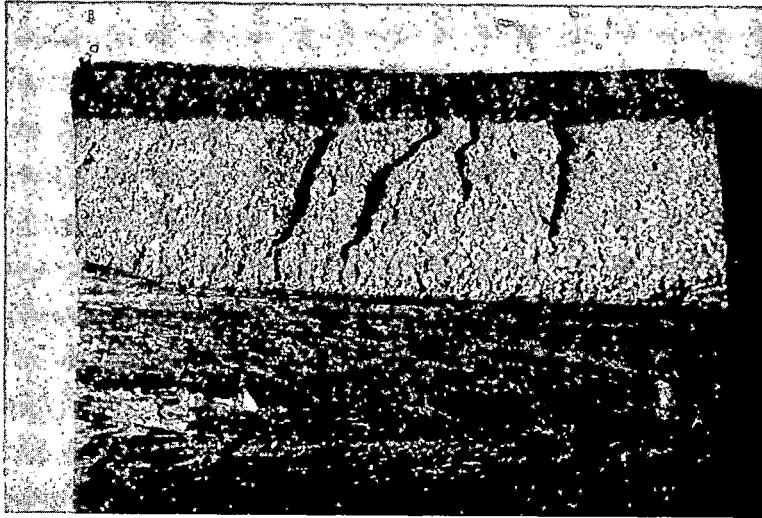


Mag. 12,000x



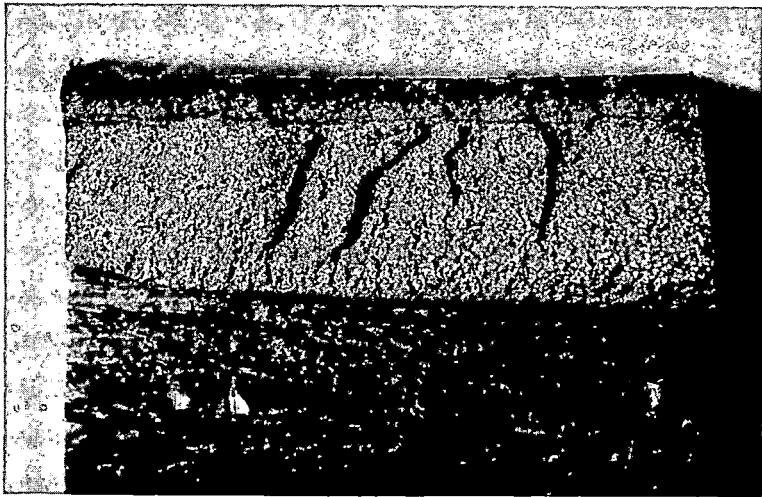
Mag. 12,000x

Figure 2-15. Thin Foil Transmission Electron Micrographs of the Reducer (Loop B) Material Showing the Fine Structure and Interlath Spacing of the Pearlite Phase



} Service crack  
} Laboratory fracture

Before cleaning



} Service crack  
} Laboratory fracture

After cleaning

Figure 2-16. Appearance of Crack Surface at 64° in Reducer B Before and After Cleaning

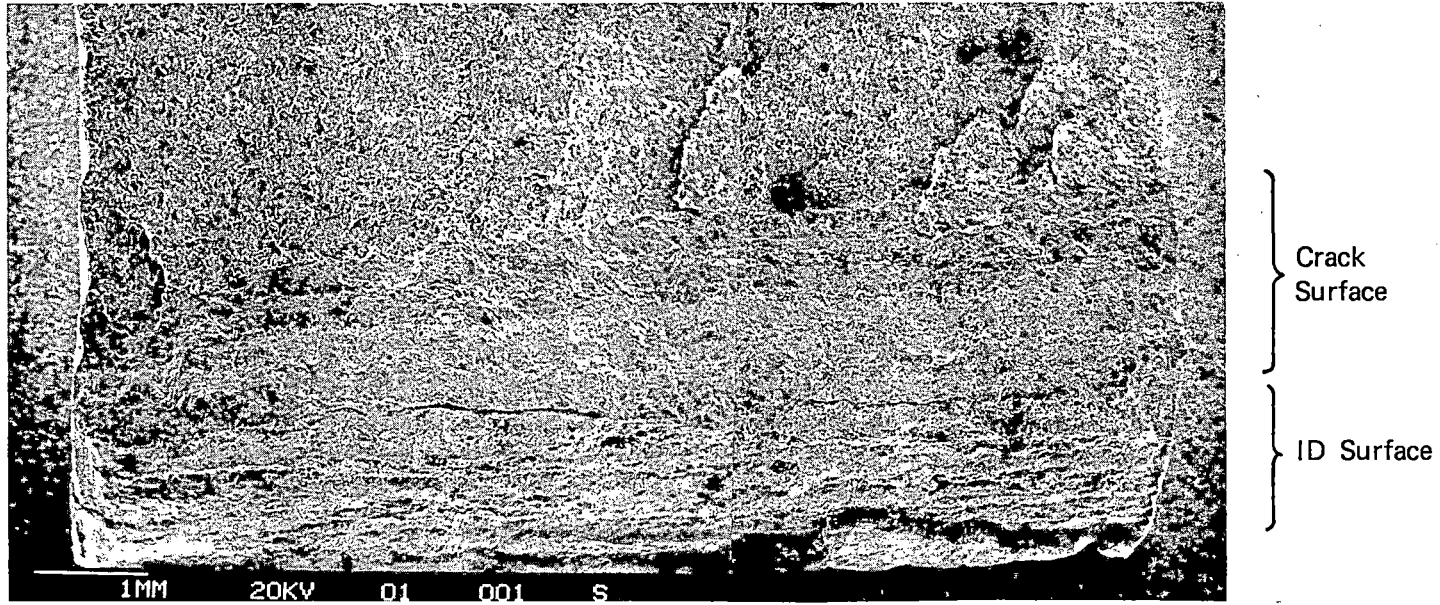
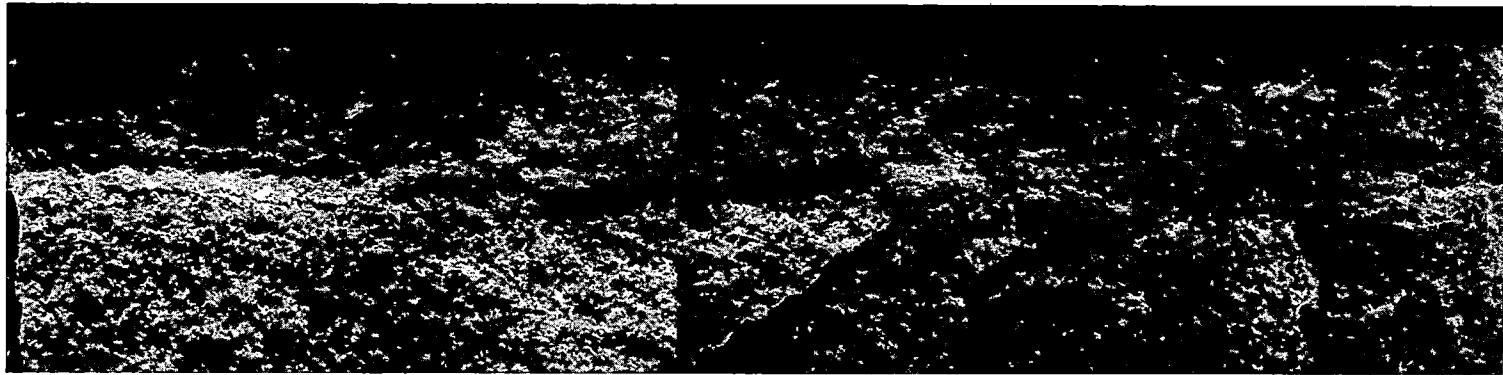


Figure 2-17. Appearance of Crack Surface at 108° in Reducer C Before Cleaning

2-22

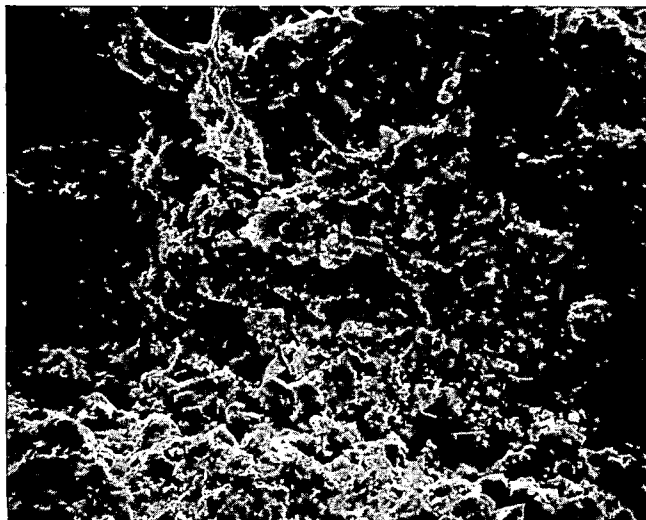


} Field crack  
} Lab. Fracture

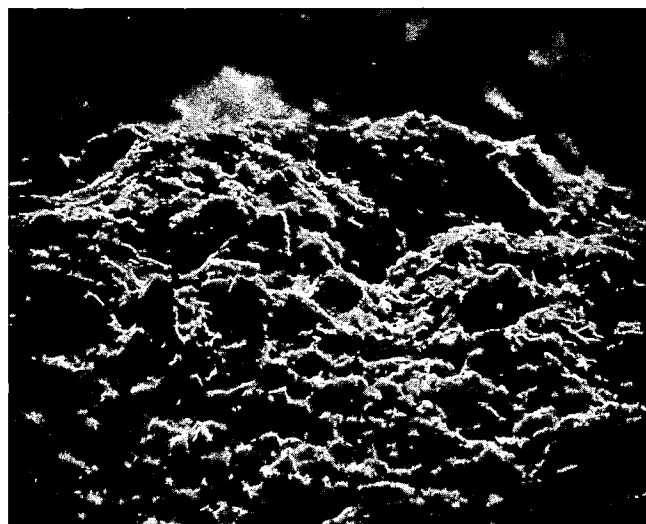
Mag. 20x

Figure 2-18. Crack Surface at 64 Degrees After Cleaning, Reducer B

15,801-18

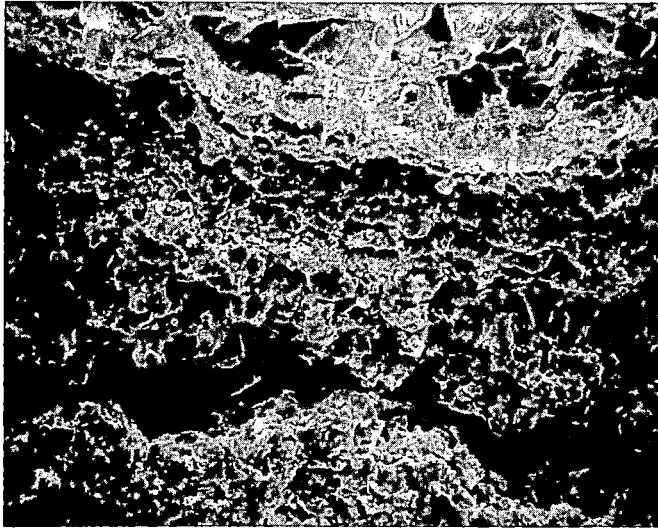


Mag. 500x

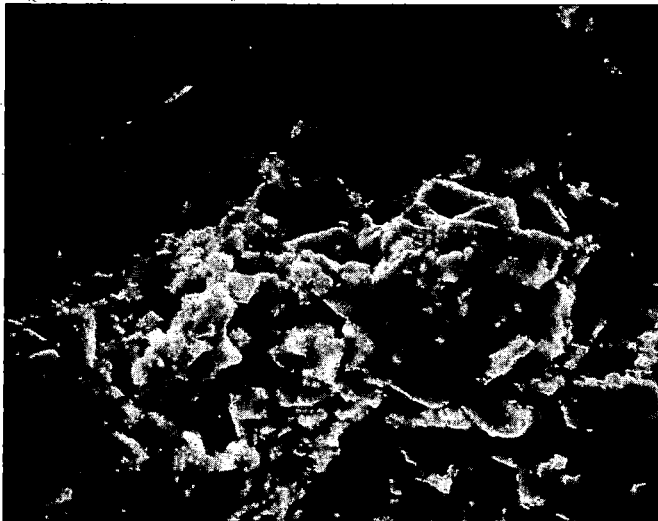


Mag. 1000x

**Figure 2-19.** Fractographs Showing the Oxidized and Corroded Surface of Crack at 64 Degrees in Reducer B

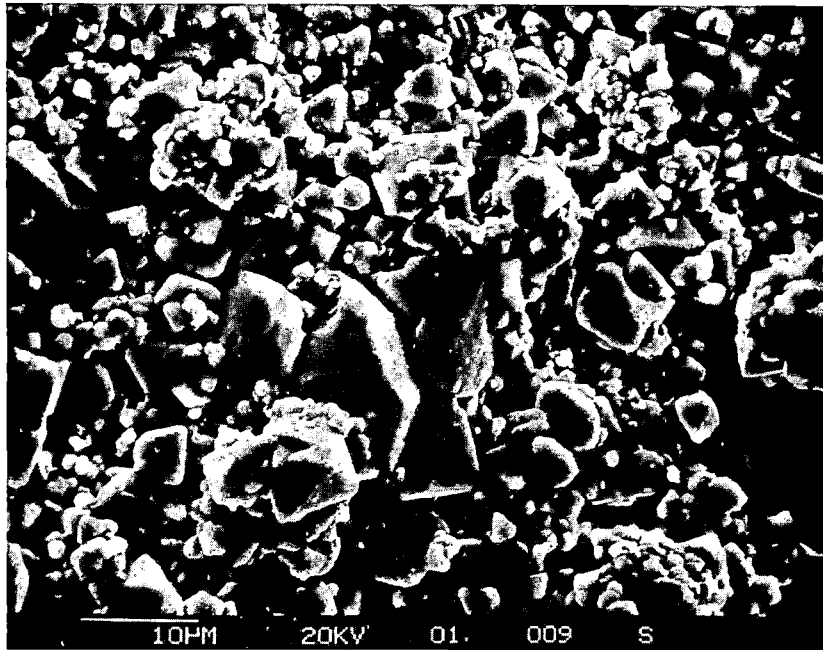


Mag. 500x

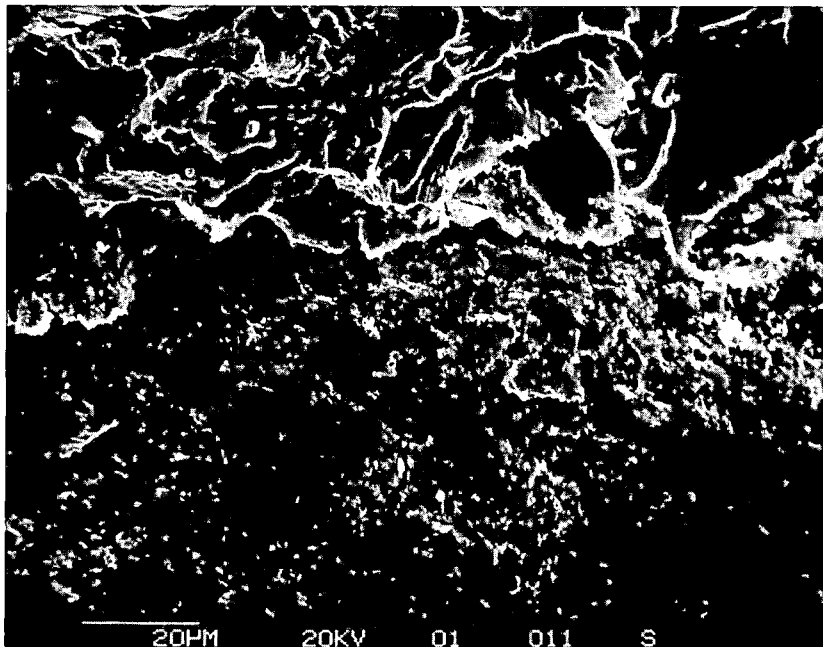


Mag. 2000x

**Figure 2-20.** Fractographic Features of Opened Crack at 64 Degrees Near Crack Tip in Reducer B. Upper photograph shows cleavage fracture produced in laboratory when the crack was opened. Note the crystalline nature of oxide.

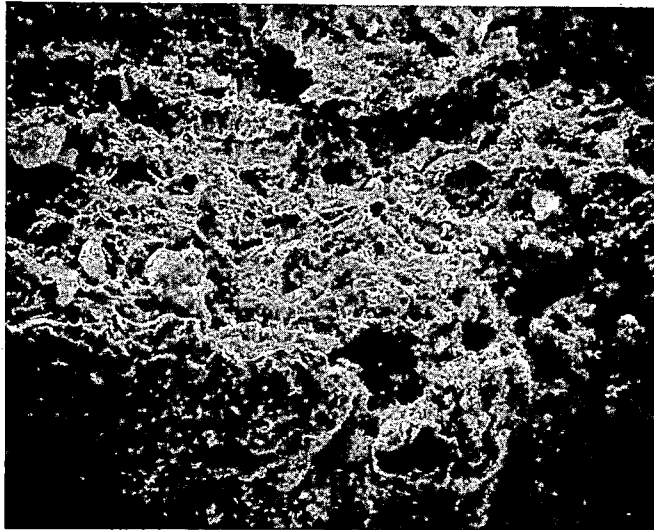


a) Oxide deposit

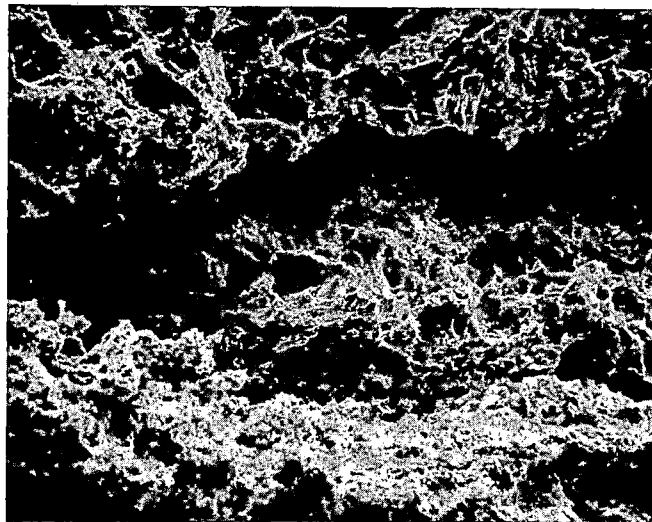


} Laboratory Fracture  
  
} Corroded surface

Figure 2-21. Fractographs Showing the Oxidized and Corroded Surface of Crack at 108 Degrees in Reducer C



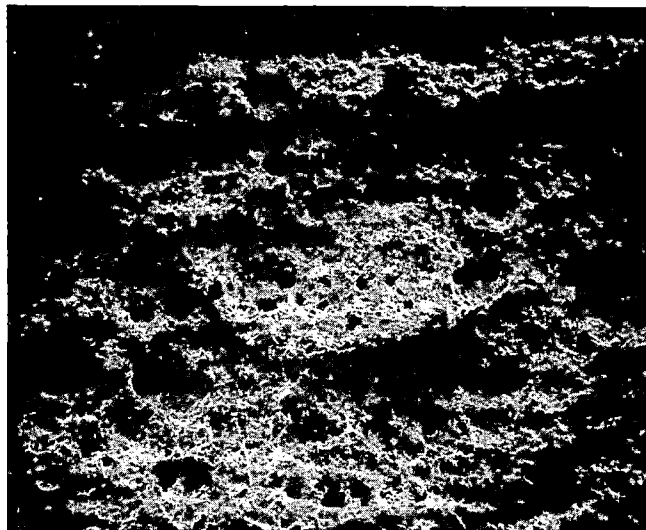
Mag. 500x



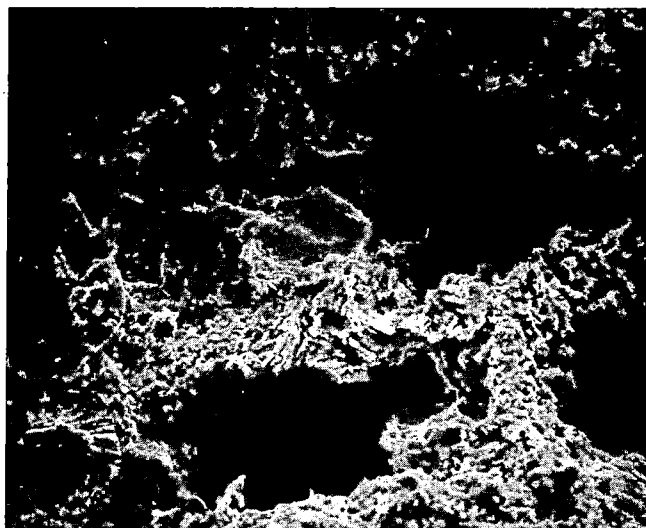
Mag. 500x

**Figure 2-22.** Fractographic Features of Cleaned Crack Surface at 64 Degrees for Reducer B



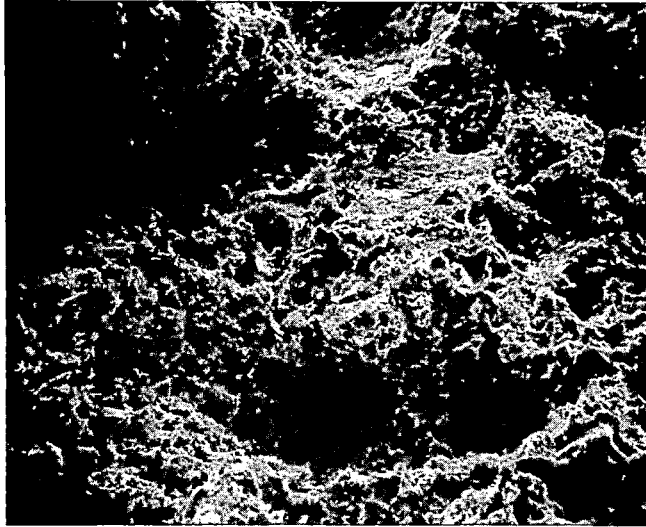


Mag. 100x

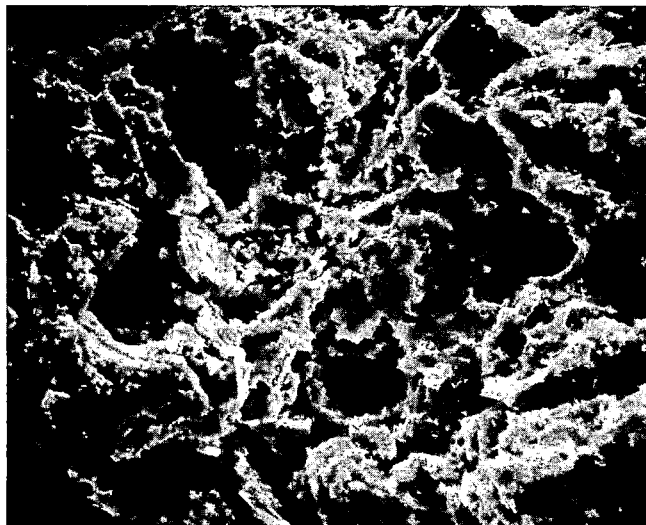


Mag. 1000x

Figure 2-23. Topographic Features of Crack Surface at 64 Degrees, Reducer B, Showing Clusters of Holes Caused by Corrosion Deoxidized by Electrolytic Cleaning

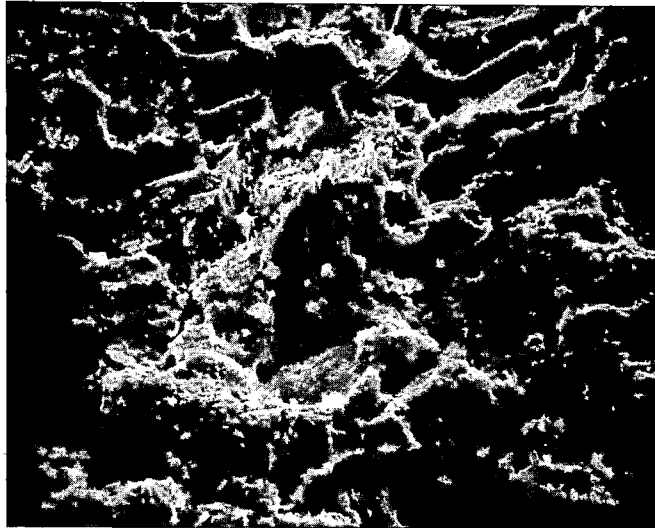


Mag. 500x

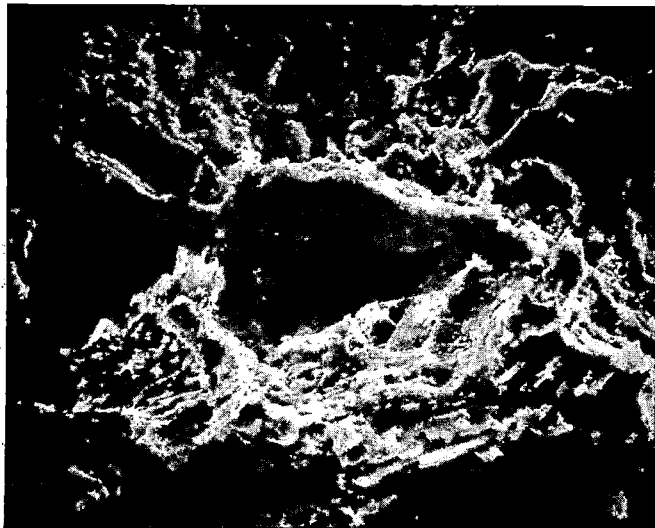


Mag. 2000x

**Figure 2-24. Fractographs Showing the Corroded Nature of the Fracture Surface at 64 Degrees, Reducer B, Surface Deoxidized by Cleaning**



Mag. 2000x



Mag. 2000x

**Figure 2-25. Fractographs of Reducer B Crack at 64 Degrees Showing a Partially Intergranular Nature of the Fracture; Deoxidized Surface**

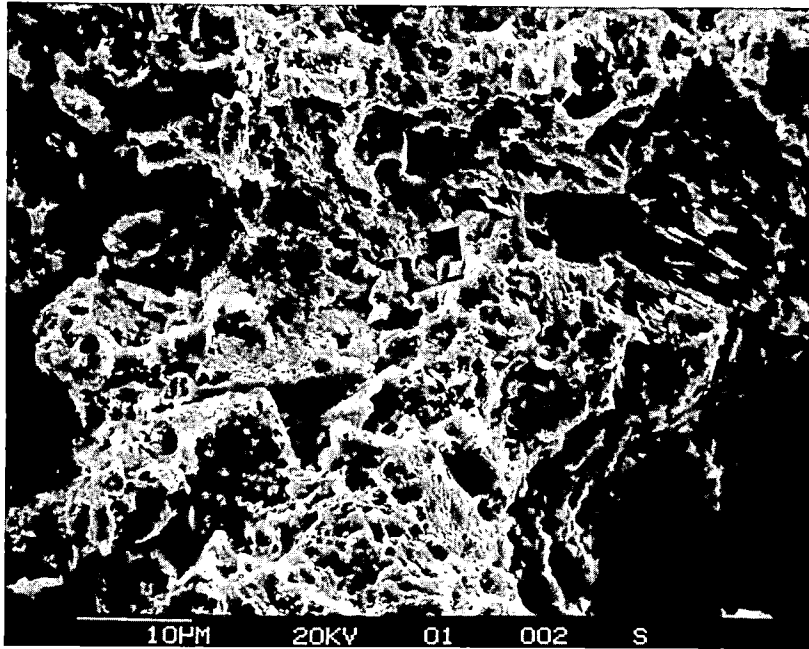
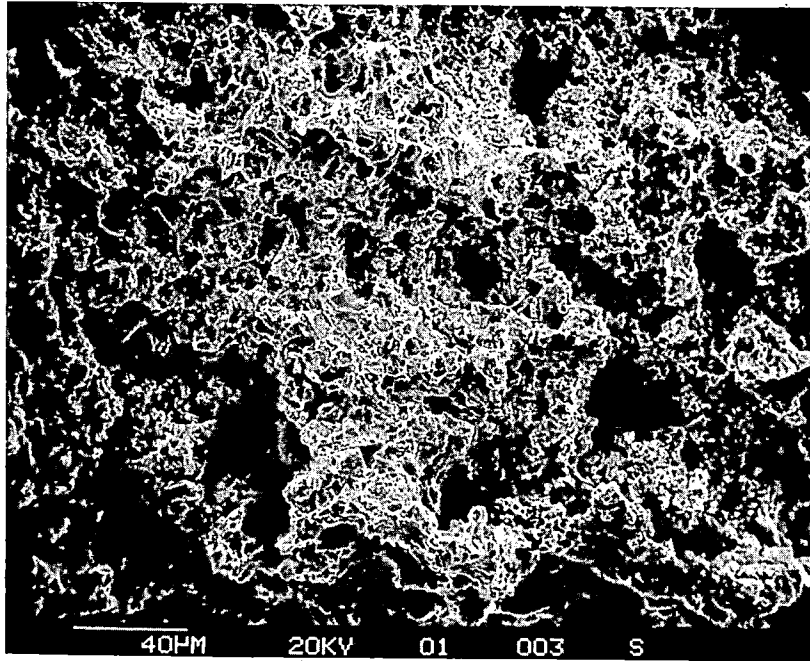
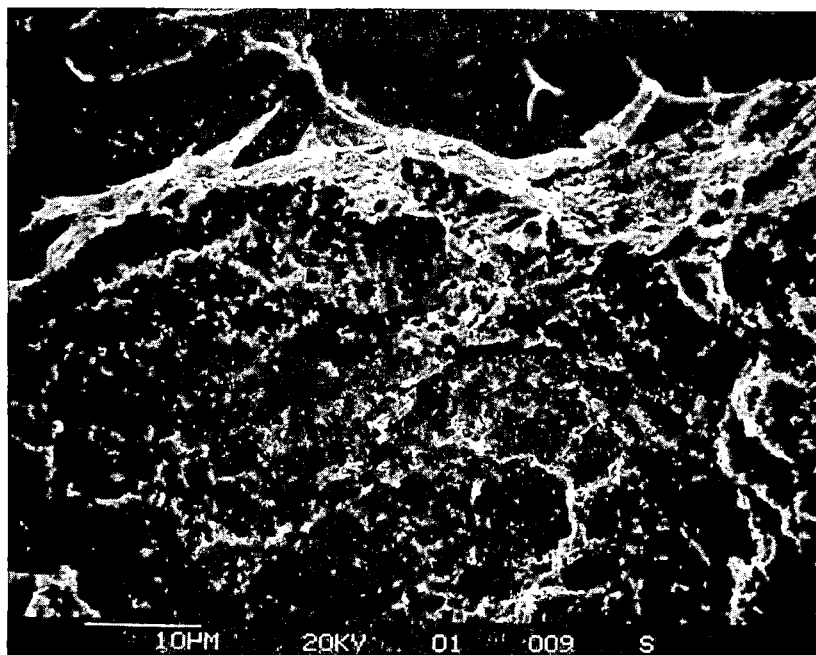


Figure 2-26. Fractographs Showing the Corroded Nature of the Crack Surface at 108 Degrees for Reducer C



} Clearance  
Overload  
Fracture

} Crack surface

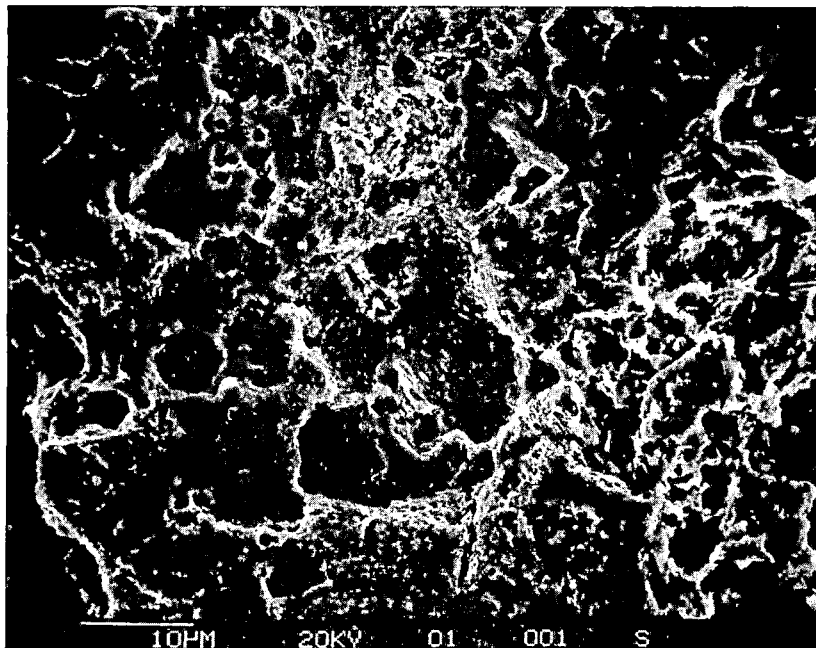


Figure 2-27. Additional Fractographic Features Seen on Crack Surface at 108 Degrees in Reducer C

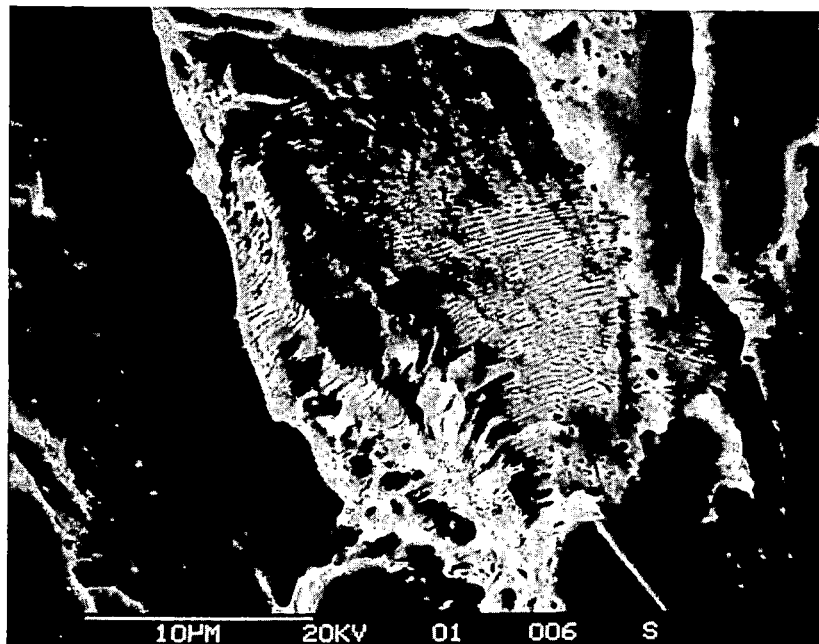
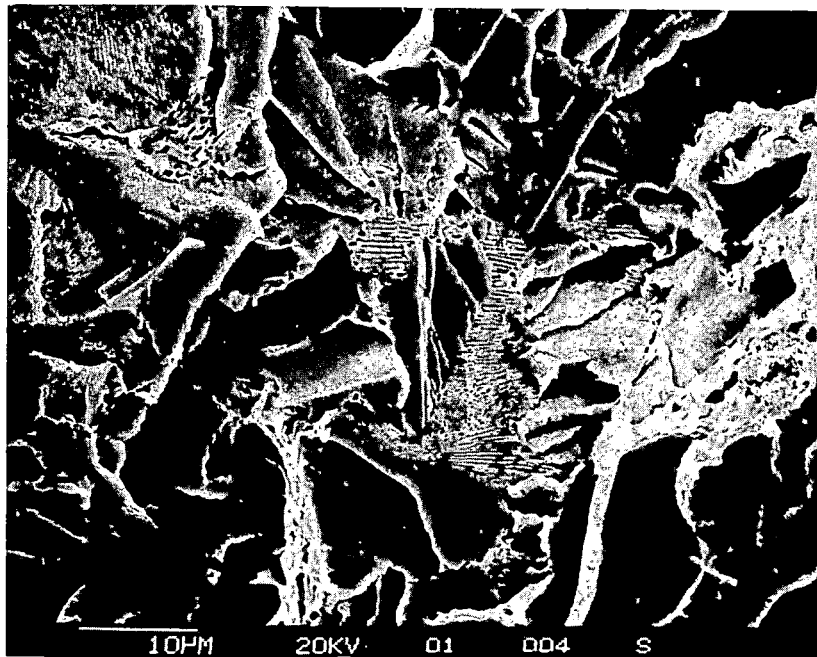
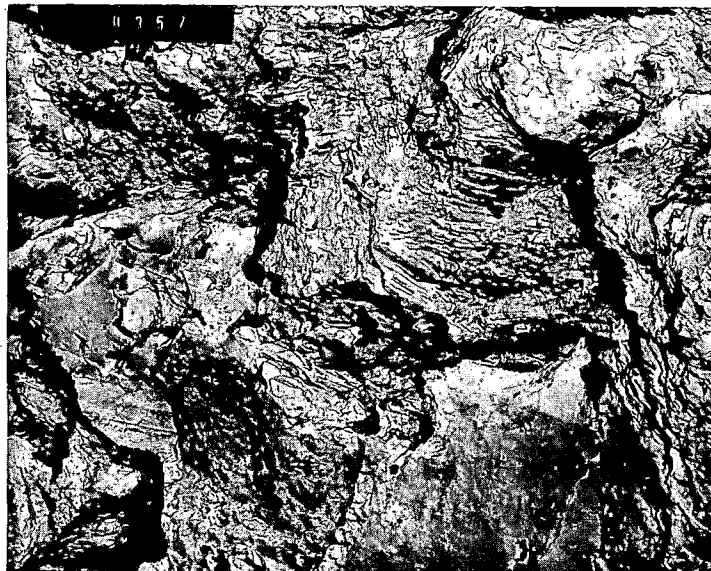


Figure 2-28. Fractographic Features Seen at the Crack-Overload Area Transition. Fracture of pearlite islands is clearly visible.



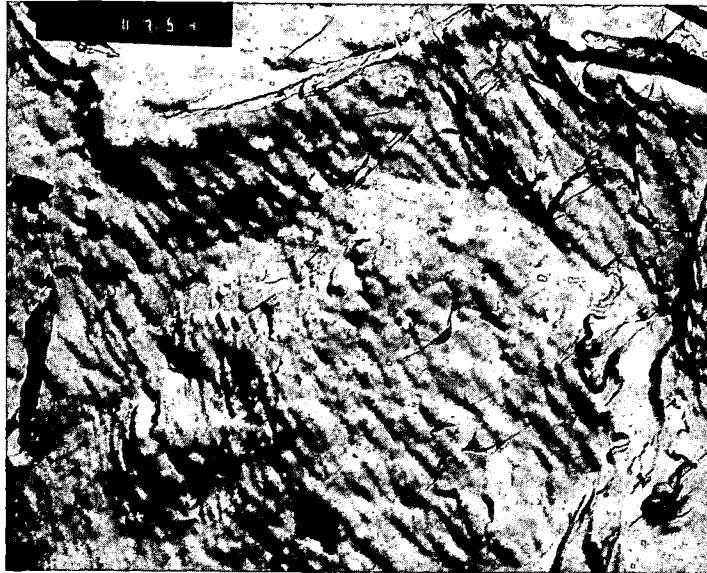
a) Fracture area

Mag. 2300x

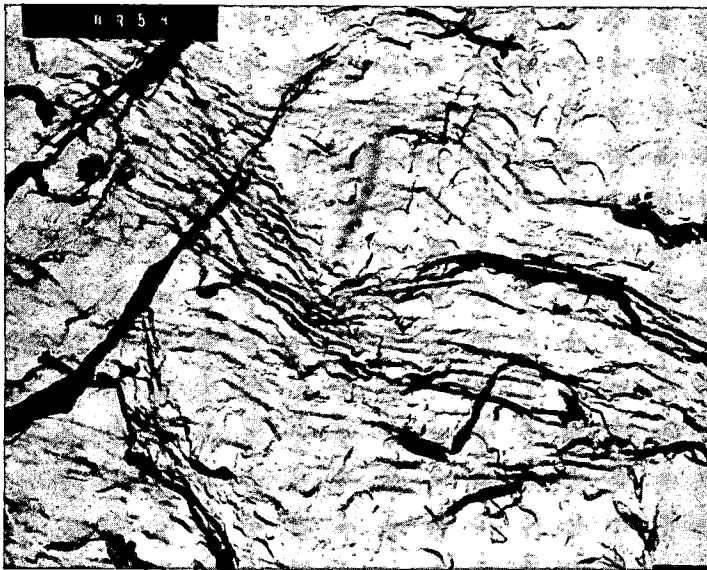
b) Overload fracture produced  
in laboratory

Mag. 2850x

**Figure 2-29.** TEM Fractographs Showing Topographic Features of Crack (a) and Overload (b) Fracture Surfaces in Reducer B at 64 Degrees. Fractograph a) depicts the corroded surface of the crack with markings produced by the fracture of pearlite colonies, while b) shows a typical brittle cleavage fracture produced at low temperature in the laboratories during opening of the crack



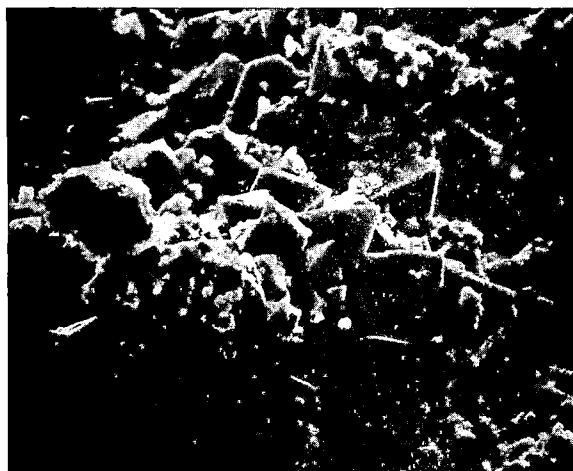
Mag. 27,000x



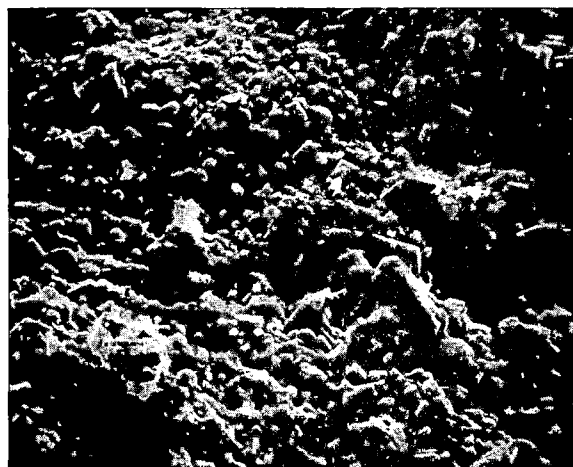
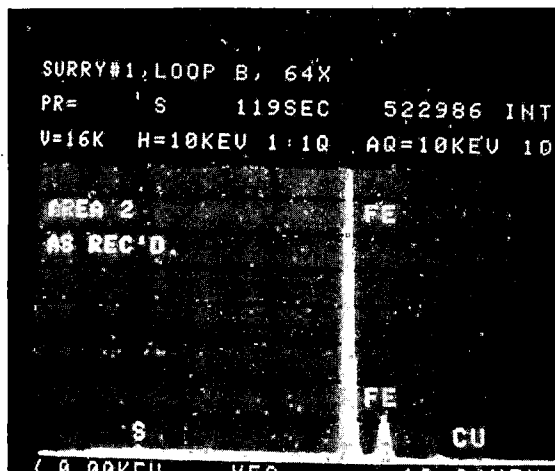
Mag. 27,000x

Figure 2-30. Fractographic Features on Reducer B Crack Surface Resembling Fatigue Striations.





Mag. 1000x



Mag. 1000x

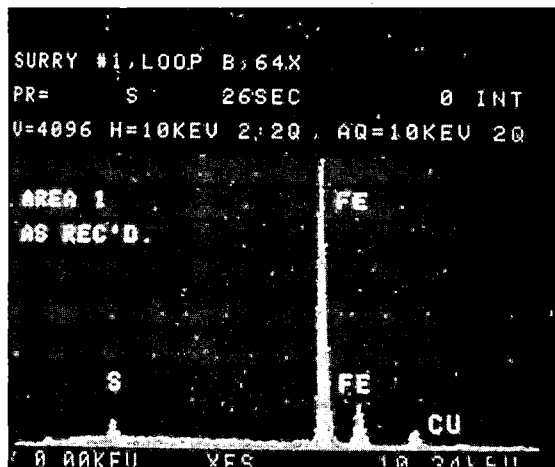


Figure 2-31. Crack Deposits Analyzed, and Output Charts of Energy Dispersive X-rays

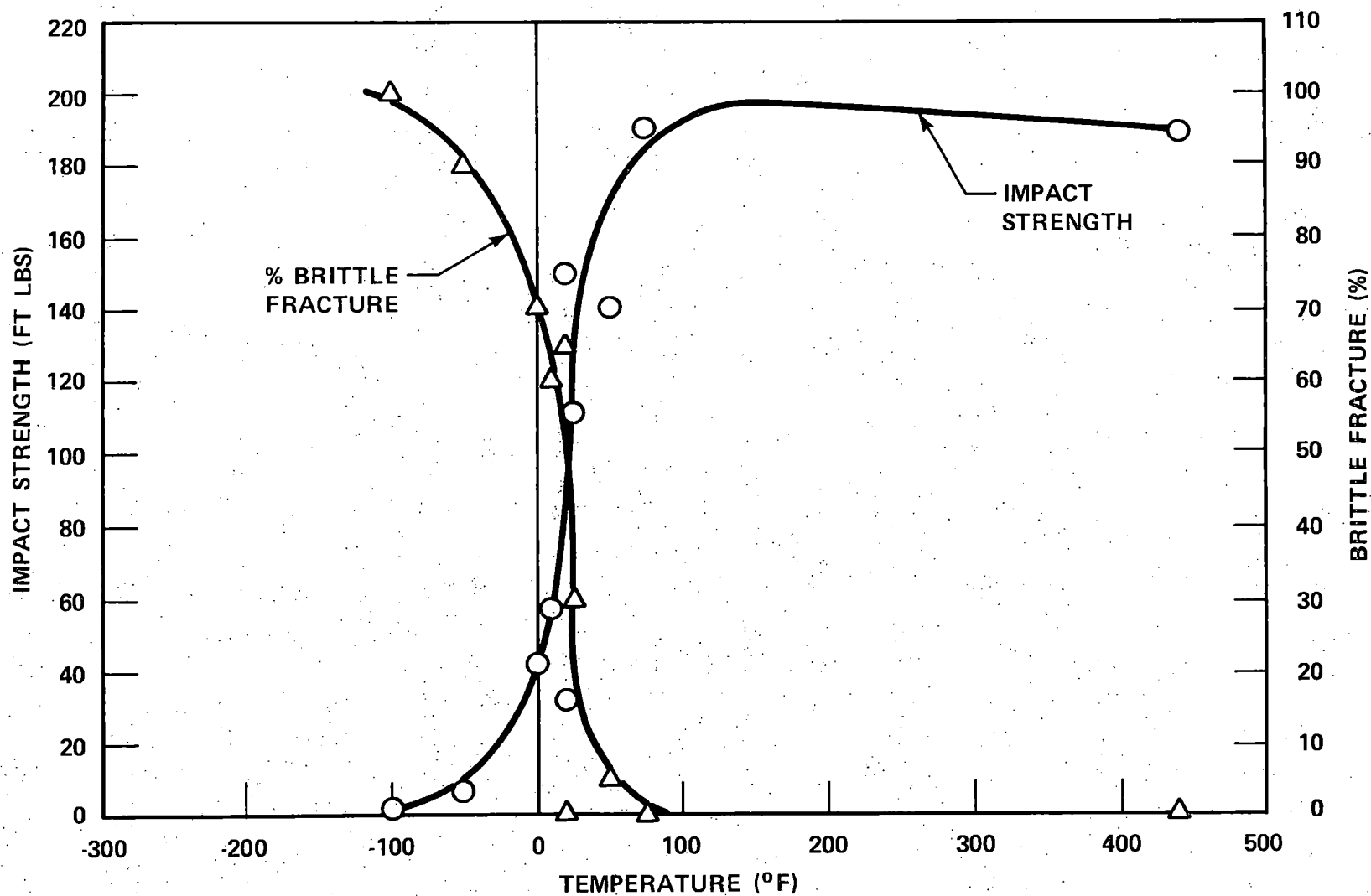


Figure 2-32. Charpy V-Notch Properties of Reducer B Material in the Test Temperature Range of 100 to 440°F

### SECTION 3

#### DISCUSSION

An examination of the chemical composition and strength properties of the Loop B reducer showed that the material conformed to the ASTM A106 Gr. B specification. No microstructural abnormalities contributing to cracking were found. The material can be considered as notch insensitive, having Charpy impact values of about 190 ft lb at room and operating temperature, and a ductile-brittle transition temperature of about 25° F.

Visual and microscopic examination of the inside surfaces of Reducer B and C sections near the nozzle-to-pipe joint revealed several cracks and pits (figures 2-1 to 2-5). The cracks tended to initiate from machining grooves or grinding marks below the "knee" of a reduced section. A piece containing the largest crack in Reducer B (figure 2-1) showed severe, continuous pitting along the crack. This crack, when opened, measured 0.080 inches and was located 121° away from the top (0°) position. The deepest crack in Reducer C measured 0.070 inches and was located at 108°. Smaller cracks were found at other locations in the reduced sections of both pipes. The cracks ran along the circumference of the pipes and grew in a relatively straight manner from the ID surface towards the OD surface (figures 2-6 to 2-11) with very little branching. The cracks were transgranular in nature and were not influenced by the banded microstructure. The walls of the cracks were severely oxidized. Bulging and narrowing of the oxide along the crack path (figures 2-5 and 2-9) suggest a crack-arrest and growth mechanism. A few beach marks, seen in figure 2-16, further point to an intermittent growth mechanism. Some of the oxidation was in the form of intrusions rather than cracks (figures 2-8 and 2-12). The relatively straight nature of cracking in the radial direction suggests that aqueous corrosion was assisted by stress. Opened cracks showed a dark corrosion product on the surface. Higher magnification fractographs showed the product to be mostly crystalline (figure 2-21), presumably  $Fe_3O_4$ . This oxide is more voluminous than the parent metal and could exert an additional stress for crack propagation. The cracking process appears to be relatively slow and perhaps self-limiting.

Although electron replica fractography indicated some regions of fracture surface resembling fatigue striations, it could not be conclusively shown that these were not the result of fracture of pearlite colonies and hence are not structure related. It is also recognized however, that any substantial evidence of fatigue striations could have been lost by the presence of

corrosion. The character of the cracks found in the Surry reducers is similar to those seen in other cracked feedwater pipes (notably the D.C. Cook Unit 1 and Palisades plants<sup>[1,2]</sup>) where fatigue striations were clearly seen on the fracture faces. Based on the evidence noted above and the similarity of the character of Surry cracks to those of the Cook and Palisades cracks, it is believed that the cracking in the Surry pipes is most likely caused by corrosion fatigue.

## **SECTION 4**

### **CONCLUSIONS**

The cause of cracking in the feedwater line reducers of Loop B and Loop C at the Surry No. 1 Station appears to be a combination of aqueous corrosion and corrosion fatigue. Contributing to crack initiation were a sharp geometrical discontinuity, machining, and grinding marks.

The material met the chemistry and strength requirements of ASTM A106 Gr. B specification. Microstructural studies indicated no abnormalities in the fine structure.

## REFERENCES

1. A. Madeyski, G. V. Rao, and T. R. Mager, "Metallurgical Investigation of Cracking in the Steam Generator Feedwater Pipes of the D. C. Cook Units 1 and 2, WCAP-9581, Westinghouse Nuclear Energy Systems, August 1979.
2. A. Madeyski, G. V. Rao, and T. R. Mager, "Metallurgical Investigation of Cracks in the Steam Generator Feedwater Pipe of the Palisades Nuclear Generating Station," WCAP-9669, Westinghouse Nuclear Energy Systems, February 1980.